



# **Magnetotelluric (MT) Data – 3D Inversion Modeling Eastern Tasmania, Australia**

**Final Report**

***Volume 1 of 1***

**Prepared for  
KUTh Energy Ltd.**

**By  
Geosystem Srl  
WesternGeco EM  
Milan, Italy**



**Effective date: October 2009**

### Revision History

Rev. No.	Effective Date	Description	Prepared by	Reviewed by	Approved by
01	16 September 2009	Initial Draft	Wolfgang Soyer	Stephen Hallinan	Stephen Hallinan
02	14 October 2009	Final Draft	Alessandra Battaglini		
03	21 October 2009	Final Draft rev. 01	Stephen Hallinan		
04	04 Nov. 2009	Final Report, with KUTH revisions			

## CONTENTS

SUMMARY .....	1
1 INTRODUCTION .....	2
2 Qualitative data analysis .....	4
2.1 Frequency range and data quality .....	4
2.2 MT “Static shift” and Time Domain EM Soundings.....	5
2.3 Tipper and Induction Vectors .....	9
2.4 MT Impedance maps and pseudo-sections.....	11
3 3D MODELING .....	14
3.1 Mesh dimensions .....	14
3.2 Topography and Bathymetry.....	16
3.3 Inversion parameters .....	17
4 3D MODEL RESULTS .....	19
4.1 Note on fill-in MT data acquisition to improve 3D model .....	20
5 BIBLIOGRAPHY .....	24
Appendix A GLOSSARY.....	A-1
Appendix B 3D MT INVERSION.....	B-1
B.1 AN INTRODUCTION TO 3D MT INVERSION .....	B-1
B.2 3D FORWARD MODELING .....	B-1
B.3 3D INVERSION .....	B-1
Appendix C PRINCIPAL 3D MODEL PARAMETERS.....	C-1
Appendix D DIGITAL DATA ON CD .....	D-1
D.1 Digital Data on CD .....	D-1
D.2 OUTPUT DATA FORMATS.....	D-1
D.2.1 Model File .....	D-2
D.2.2 Predicted Data.....	D-2
D.2.3 Inversion Log and Error File .....	D-2
Appendix E Maps and Cross Sections.....	E-1
E.1 maps .....	E-1
E.2 cross sections .....	E-1

**FIGURES:**

Figure 1	3D views of resistivity cross-sections through main profiles “A”, “B” and “C” .....	1
Figure 2:	MT Survey location in Eastern Tasmania (Google Earth). .....	2
Figure 3.	MT station and profile locations on topographic base map.....	3
Figure 4.	Example soundings STL022A, EWA016A (upper panel) and NSB034A & NSA042A (lower panel). Data are rotated to N106°E, the rotation angle for the 3D modelling. Off-diagonal components xy (red) and yx (blue) are displayed in bold colours, on diagonal tensor elements are in faint colours (xx and yy). Static shift is discussed in following section.....	4
Figure 5:	Example TDEM soundings for sites: STL016A, NSOC03A, and EWOB02A, showing apparent resistivities (left), and 1D smooth and layered inversion models (right), together with model responses. Late time data are not masked, and deeper resistivity models are not reliable. ....	7
Figure 6:	MT Soundings STL031A, STL032A, and STL034A – polarizations TE (red) and TM (blue). Rotation angle here is N23°E. Green lines are synthetic responses from the 1D TDEM inversion models. MT soundings here are not corrected for static shift. Note that TDEM soundings do not always indicated a good reference for true near surface resistivity: MT and TDEM resistivities agree well for site STL032A. For STL034A, lower resistivities as sounded through MT are indicated by the TDEM results – which can be assumed right considering lower values at the relatively close site 32 (~2km distance). For site STL031A, MT data show a strong shift – nearly one order of magnitude, but the resistivity level indicated by TDEM may be overestimating the real near surface resistivity. Generally, the TDEM yields reliable results over more conductive ground.....	8
Figure 7:	Real induction vectors for 1Hz, 0.1Hz and 0.01Hz (top to bottom). Arrows are plotted in the convention pointing towards conductors. Pink arrows added to the 1Hz display show how high conductivity is indicated at major fault locations. The dashed ellipse roughly marks the location of deep high conductivity as indicated by the vectors.....	10
Figure 8	Impedance phase Invariant for frequencies 100Hz, 10Hz, 1Hz, and 0.1Hz. ....	11
Figure 9	Apparent resistivity and phase pseudo-sections for profile A. Top: TE mode, bottom: TM mode. Data rotation is N18°E, i.e. TE corresponds to electric crossline direction. Vertical stripes in the gridded apparent resistivity data reflect the significant static shifts in the data – lateral phase variation however is smooth. Very low phases and high resistivity at longest periods in the TM polarization is likely at least partly related to the coast effect. ....	12



Figure 10	Phase pseudo-sections for profile B for TE (top) and TM polarization (bottom). Data rotation is N-70°E, i.e. TE corresponds to electric crossline direction. ....	12
Figure 11	Phase pseudo-sections for profile C for TE (top) and TM polarization (bottom). Data rotation is N-73°E, i.e. TE corresponds to electric crossline direction. ....	13
Figure 12.	Plan views of full 3D model meshes (LHS) and fine mesh centred on MT station locations (RHS). Background grid is topography (SRTM DEM). The top row shows the fine 3D inversion grid, the bottom the coarser grid.....	15
Figure 13	Section views of full and core 3D model mesh (LHS, RHS), showing also the intersection with the elevation grid (RHS; fine model mesh shown here only).....	15
Figure 14	MT station locations and bathymetry. ....	16
Figure 15	Cross-section through start model of MT inversion. The ocean is coarsely discretized in the eastern padding part of the model. ....	16
Figure 16	Example MT soundings STL022A and NSB034A, showing fit between observed (LHS) and calculated 3D model response (RHS). Data rotation: 106°. Note the final resistivity model reproduces the static shifts inherent in the MT data at NSB034A, both through inclusion of near-surface structure and direct static shift factors. ....	18
Figure 17	Resistivity depth maps at 0, -1500 and -3000m msl from 3D MT inversion model 06 (fine grid, left panels) and model 102 (coarse grid, right panels). ....	19
Figure 18	Cross section along profile “A” through the 3D resistivity model 06 (fine grid, W to E, top) and model 102 (coarse grid, W to E, bottom). ....	21
Figure 19	Cross section along profile “B” through the 3D resistivity model 06 (fine grid, W to E, top) and model 102 (coarse grid, W to E, bottom). ....	22
Figure 20	Cross section along profile “C” through the 3D resistivity model 06 (fine grid, W to E, top) and model 102 (coarse grid, W to E, bottom). ....	23



## SUMMARY

Under agreement with KUTh Energy Ltd., WesternGeco's Land EM group Geosystem carried out full tensor 3D inversion modelling of a passive magnetotelluric (MT) data set from 2008-2009, comprising 201 soundings in eastern Tasmania. The data are mostly located along three profiles at nominally 1km spacing, while a subset of sites at larger spacing (ca. 10km) provides some 3D coverage and information off the lines. Additionally provided single loop time domain EM (TDEM) data were converted into WinGLink compatible format and modelled for 1D near surface resistivity distribution to estimate MT static shift effects.

The data were inverted for resistivity structure by 3D MT inversion modeling in two parallel approaches:

- i. A fine 3D grid for a detailed inversion to include 196 of the 201 soundings, where many cells between the profiles are not sampled by MT soundings.
- ii. A coarse 3D grid and reduced, more equally distributed data (62 soundings), lower frequencies, in order to minimize any false detailed structure in the fine mesh between profiles, and test for overall structure consistency of the fine mesh.

3D inversion results on the fine grid are unsurprisingly most reliable along the profiles (Figure 1 below) but poorly controlled detailed structure between, leading to a survey footprint on the results. The coarse mesh shows similar behaviour, but less so and overall consistency of the major structure is good.

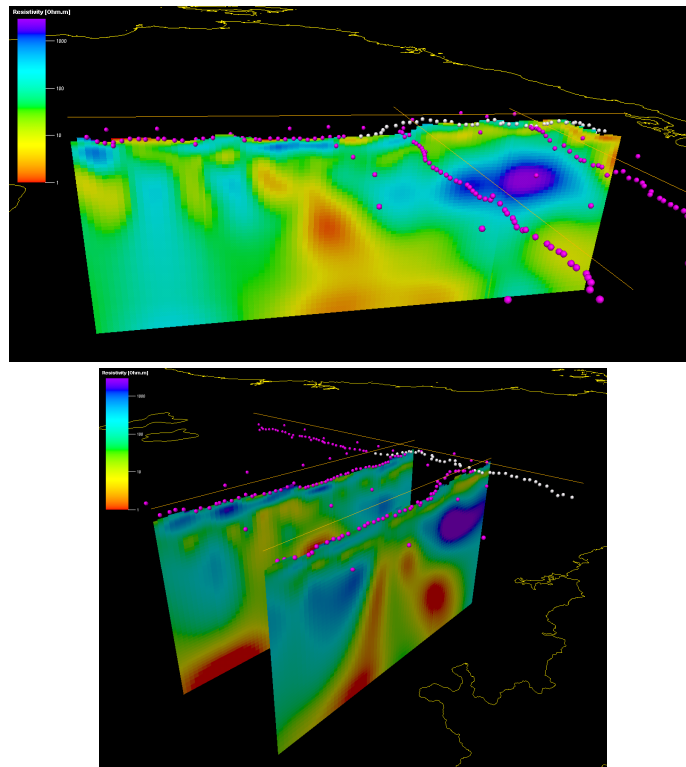


Figure 1 3D views of resistivity cross-sections through main profiles "A", "B" and "C".

The dipping conductor diagonally intersecting the study area from NW to SE is coincident with the fault zones, and possibly with a deep conductive root.

## 1 INTRODUCTION

An MT survey of in total 201 stations was carried out in eastern Tasmania in 2008 and 2009. Acquisition and data processing was conducted by Moombarriga Geoscience using MTU-5A broadband electromagnetic receivers and MTC-50 magnetic sensors. Most sounding locations are aligned along three profiles: two sub-parallel lines of about 52 km length in SSW-NNE direction, and a longer 75 km profile in WNW-ESE direction (Figure 3). Station spacing along these lines is nominally 1 km. About 25 sites located between and around the profiles provide the further spatial data information for a 3D investigation of the data set.

At 191 of the 201 MT sounding locations, single loop time domain transient measurements were additionally performed to obtain near surface resistivity information, which can serve as a control when estimating static shift inherent in the MT soundings.



Figure 2: MT Survey location in Eastern Tasmania (Google Earth).

All coordinates on maps and data in this report are given in WGS-84, UTM projection.

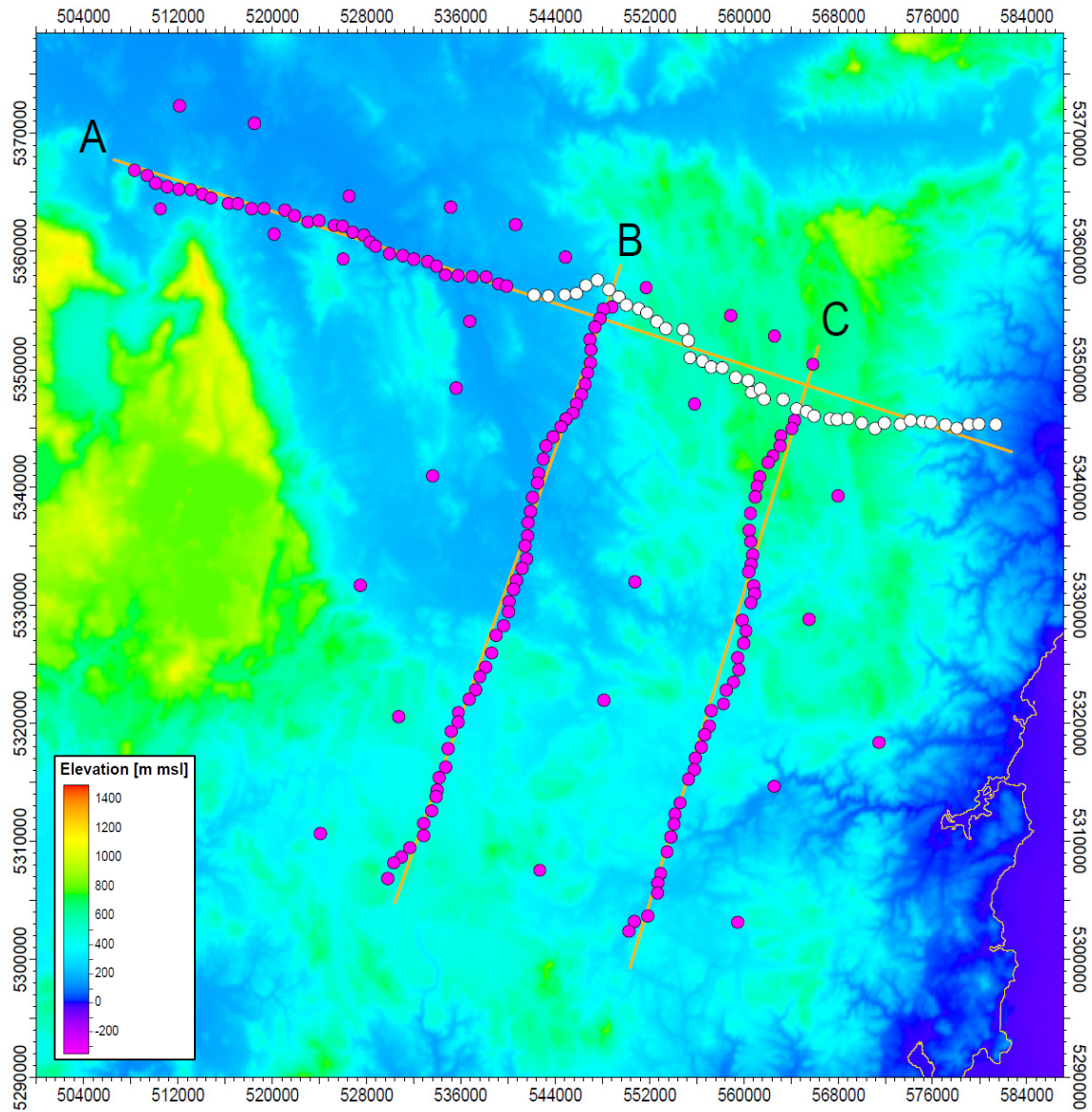


Figure 3. MT station and profile locations on topographic base map.

## 2 QUALITATIVE DATA ANALYSIS

### 2.1 Frequency range and data quality

The frequency range covered by the MT soundings is from 300Hz to over one thousand seconds in the best cases. Overall data quality is good, and careful data editing by masking poorer data sections was necessary prior to 3D inversion (illustrated in Figure 4).

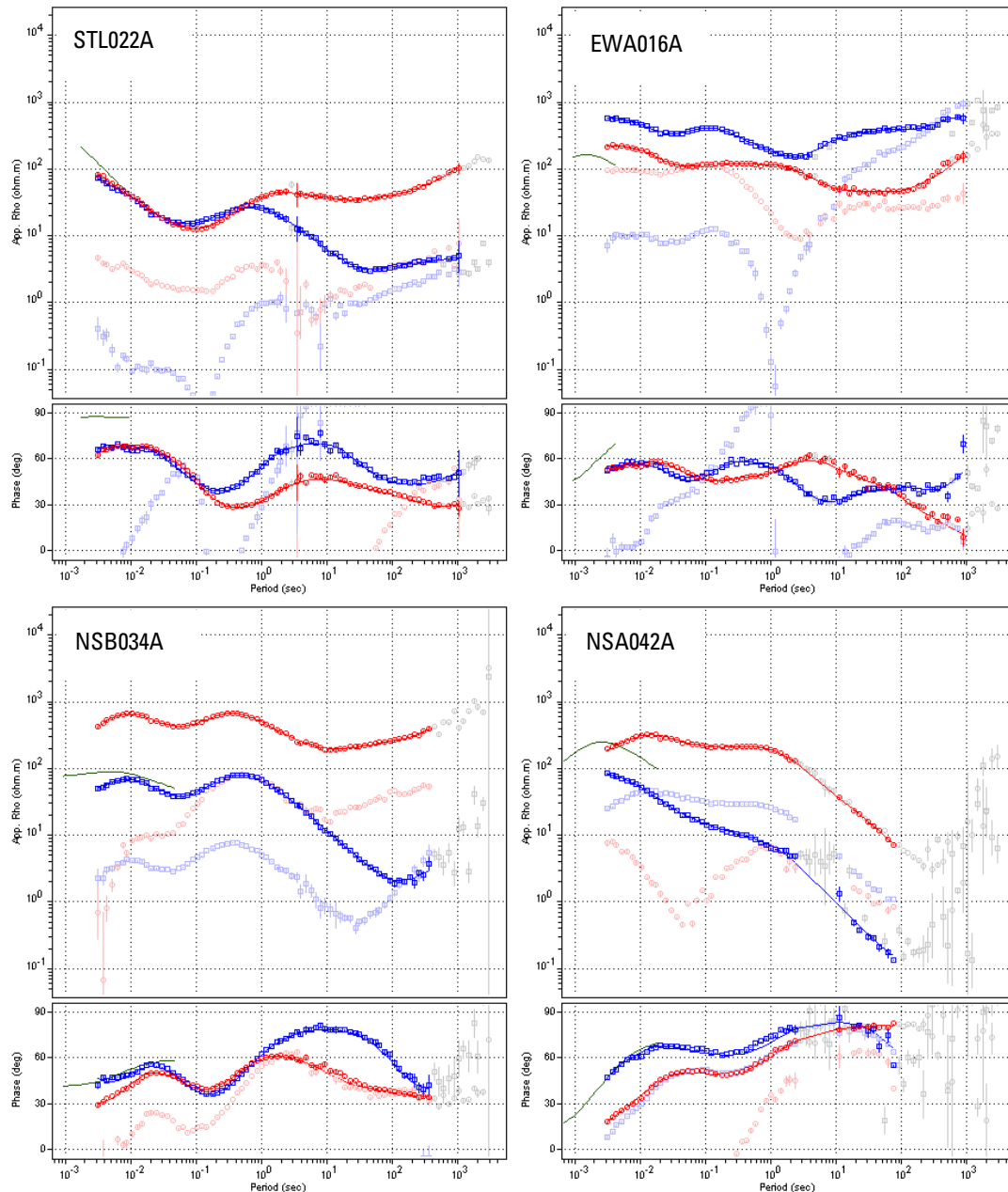


Figure 4. Example soundings STL022A, EWA016A (upper panel) and NSB034A & NSA042A (lower panel). Data are rotated to N106°E, the rotation angle for the 3D modelling. Off-diagonal components xy (red) and yx (blue) are displayed in bold colours, on diagonal tensor elements are in faint colours (xx and yy). Static shift is discussed in following section.



## 2.2 MT “Static shift” and Time Domain EM Soundings

Statics are prevalent in the current MT data set; MT apparent resistivity curve splits due to telluric distortion effects generally caused by topography and near surface resistivity change. The phase curves on the other hand should not reflect these distortions (e.g. Figure 4). There are several ways in dealing with static shifts inherent in MT (e.g. discussion in Soyer et al., 2008):

1. Let the static factors be reproduced by near surface topography and structure modelled by the inversion (3D and 2D TM mode).
2. Invert for static shift factors directly as an inversion parameter (2D, 3D)
3. “Manually” adjust static shift factors before inverting, either by:
  - a. Using non MT information, e.g. TDEM results, or
  - b. Estimating the true level of resistivity from neighbouring sites’ information, e.g. from pseudo-section displays, iteratively removing statics until smooth sections are obtained.

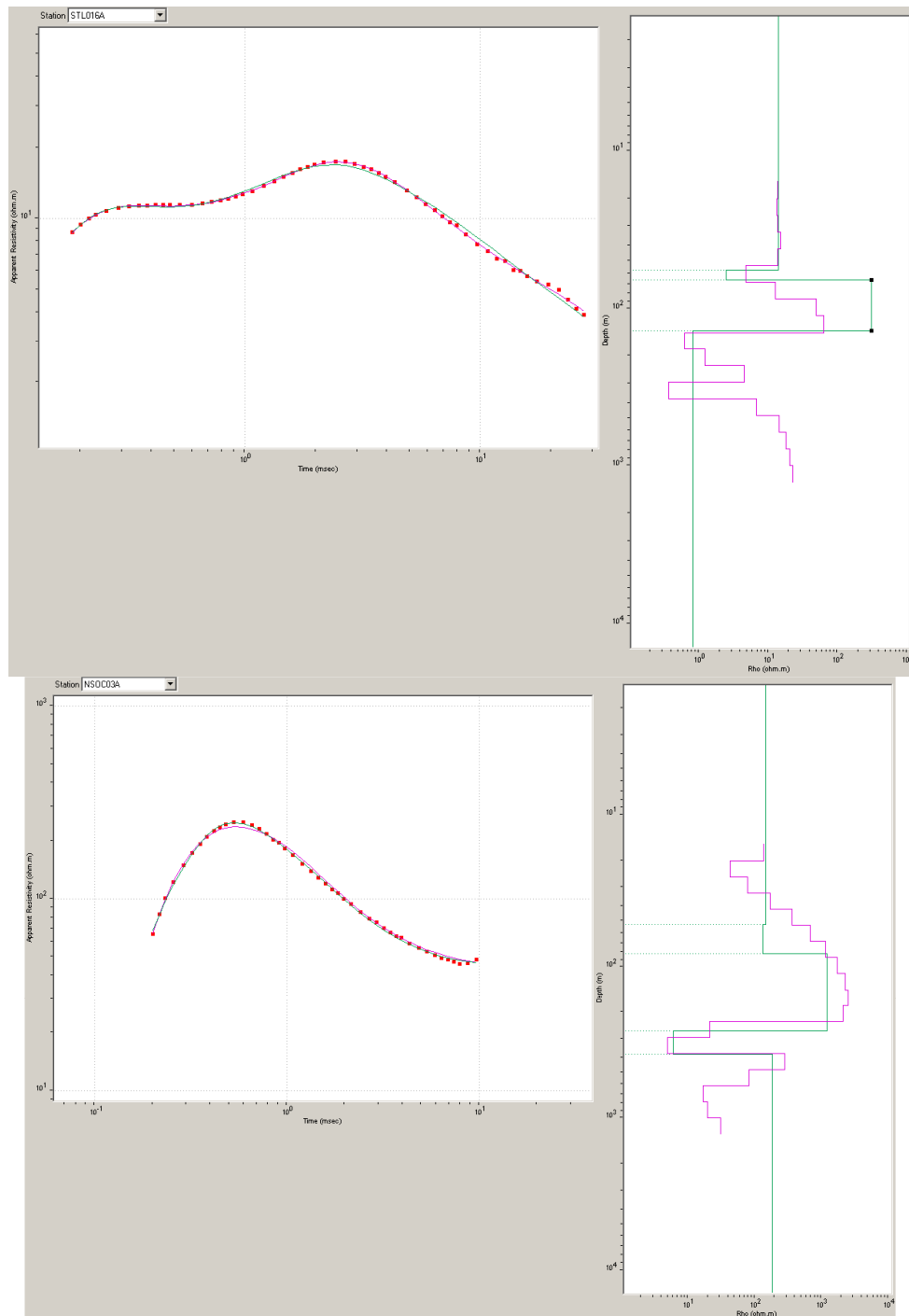
Since the TDEM method involves only magnetic fields (both transmission and reception), the soundings can generally be expected to be little affected by moderate, lateral near surface resistivity contrasts, and TDEM data have been commonly employed in past MT surveys. Coincident Loop TDEM data, particularly from Single Loop mode offered by Sirotem and TerraTem (used here), provide optimum resistivity data in conductive environments where the inductive response is well behaved, but not on resistive outcrop, however, such as massive limestone or fresh volcanics, crystalline basement etc., where the response is well predicted, and the voltage decay curves are more often distorted. Typically this results in a false “conductive” response. The data need to be treated carefully therefore before using for MT static shift. (Geosystem has used the Sirotems for over 15 years, and opts for In-Loop TDEM solutions if the terrain is resistive; significantly resistive terrain however will still require larger transmitter loops to get correct behaviour.)

TDEM soundings in this MT survey were conducted deploying a TerraTem system in a single loop setup configuration. Data were provided in one version of the Amira ASCII format. Files containing the data time windows after the current switch were provided in a separate file.

A conversion routine was implemented to re-write the data set into the Geosystem WinGLink TEM format, additionally adding the relevant information on the repetition rate.

Data were loaded into the WinGLink data base, and 1D inversions subsequently conducted – both smooth Occam type inversions, with 18 logarithmically equi-spaced layers, and discrete models of usually four layers.

Time windows covered by the data set is between 0.1 and 10 msec, covering a depth range of sensitivity from about ten meter down to a few hundred meters. Example soundings are displayed in Figure 5. The earlier time data and resistivity models in the upper 200m are reasonable. The later time data are noisier, and thus the inverted resistivities from deeper horizons are unreliable, creating false conductors and resistors in the automatic modeling. Manual, depth limited modeling results from data where late time data are masked are more reliable.





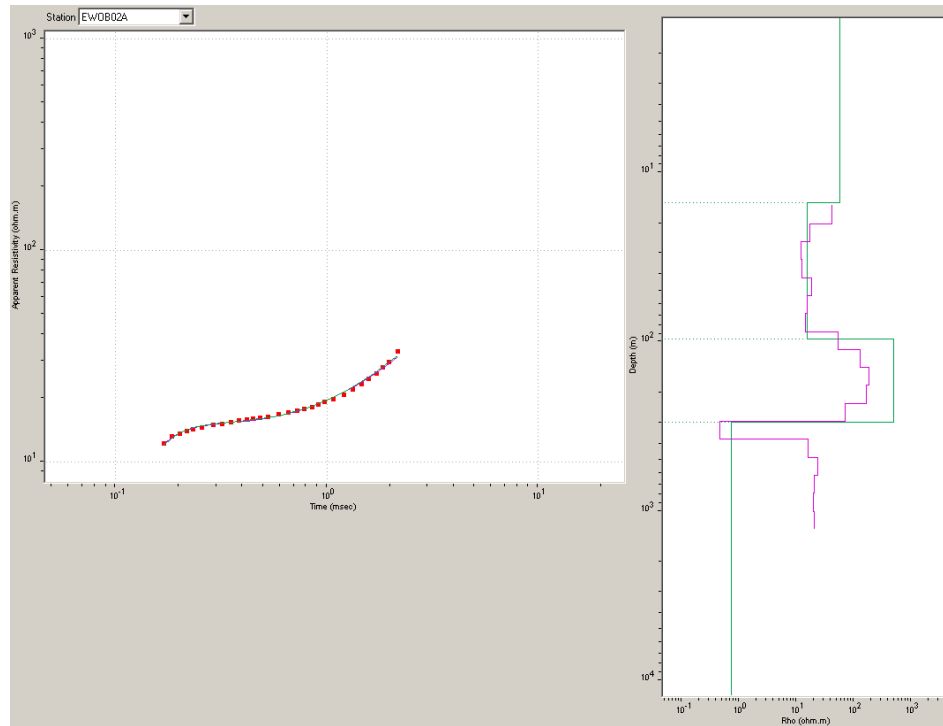


Figure 5: Example TDEM soundings for sites: STL016A, NSOC03A, and EWOB02A, showing apparent resistivities (left), and 1D smooth and layered inversion models (right), together with model responses. Late time data are not masked, and deeper resistivity models are not reliable.

From the 1D inversion results (layered models), magnetotelluric forward responses were calculated for the TDEM soundings were reasonable 1D models could be obtained. The resulting synthetic MT responses are illustrated with the measured MT data, and provide an indication on the true near surface resistivity level at the MT site locations and thus an estimate on the static shift factors encountered in the MT soundings.

Figure 6 gives an impression on the validity of this calibration approach – here again in a comparably resistive setting.

Finally, the approach used in this study was to model the MT static shift in the 3D inversion.

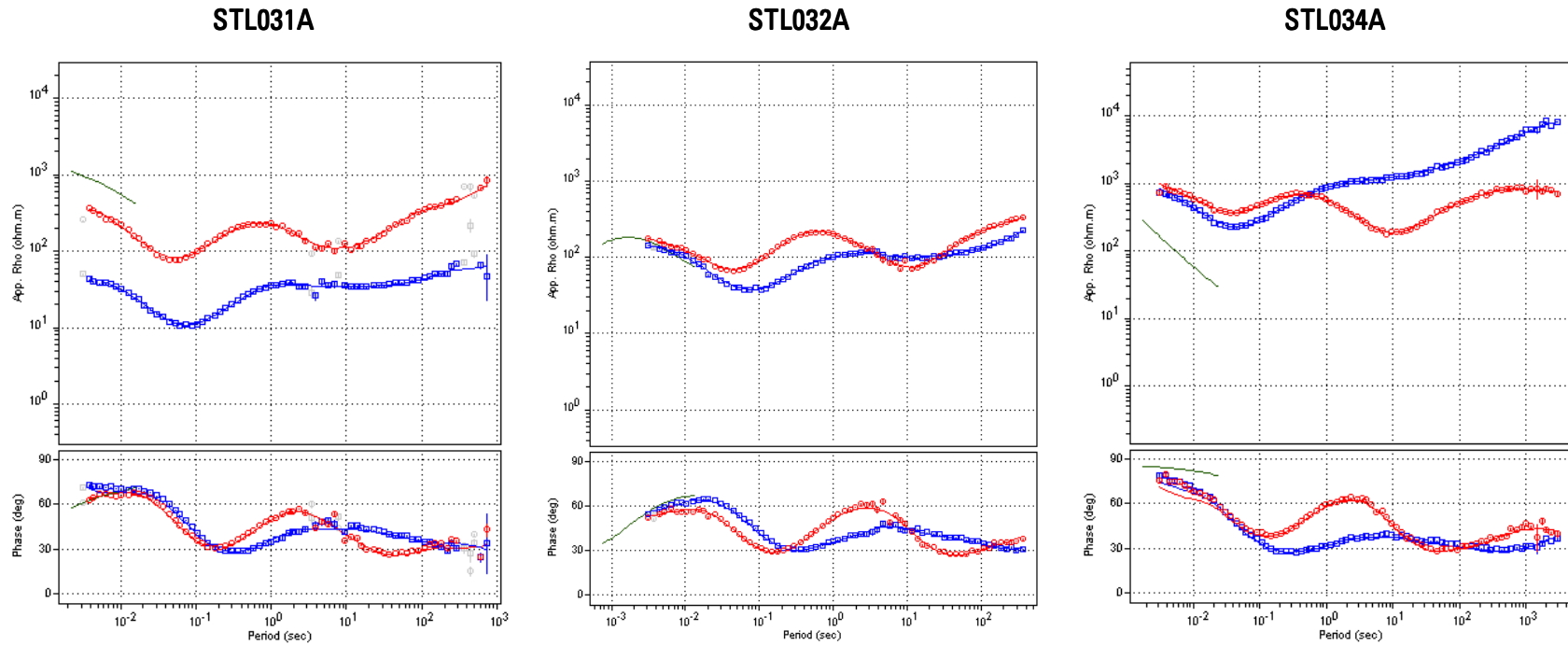
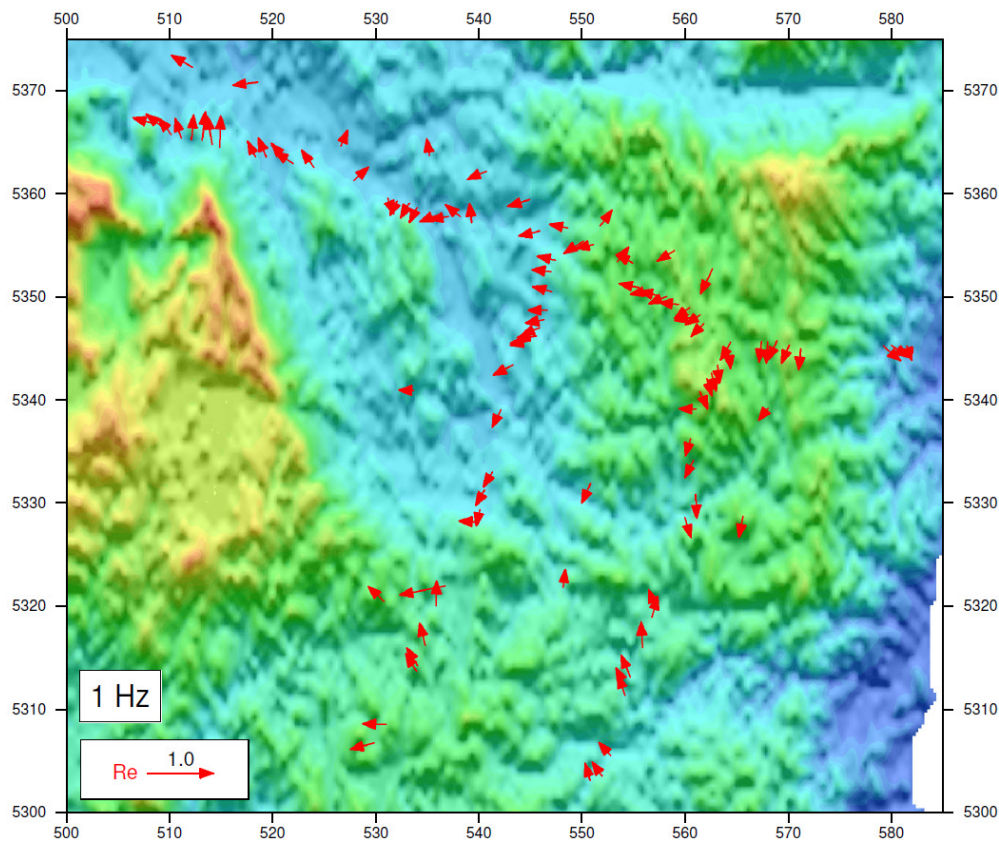


Figure 6: MT Soundings STL031A, STL032A, and STL034A – polarizations TE (red) and TM (blue). Rotation angle here is N23°E. Green lines are synthetic responses from the 1D TDEM inversion models. MT soundings here are not corrected for static shift. Note that TDEM soundings do not always indicated a good reference for true near surface resistivity: MT and TDEM resistivities agree well for site STL032A. For STL034A, lower resistivities as sounded through MT are indicated by the TDEM results – which can be assumed right considering lower values at the relatively close site 32 (~2km distance). For site STL031A, MT data show a strong shift – nearly one order of magnitude, but the resistivity level indicated by TDEM may be overestimating the real near surface resistivity. Generally, the TDEM yields reliable results over more conductive ground.

### 2.3 Tipper and Induction Vectors

Slightly over half of the MT sites contain magnetic tipper data – i.e. transfer functions between vertical and horizontal magnetic field components.

Illustrated as induction vectors, these give insight into lateral conductivity changes: in Figure 7 real parts of these vectors are displayed for frequencies 1Hz, 0.1Hz and 0.01Hz in the reverse convention i.e. pointing towards conductors. At 1Hz and partly 0.1Hz, a clear correlation between structural faults, as can be inferred from the shaded relief map and the orientation of vectors can be observed. Towards longer periods, an extended high conductivity zone crossing the survey area in NW-SE direction is indicated.



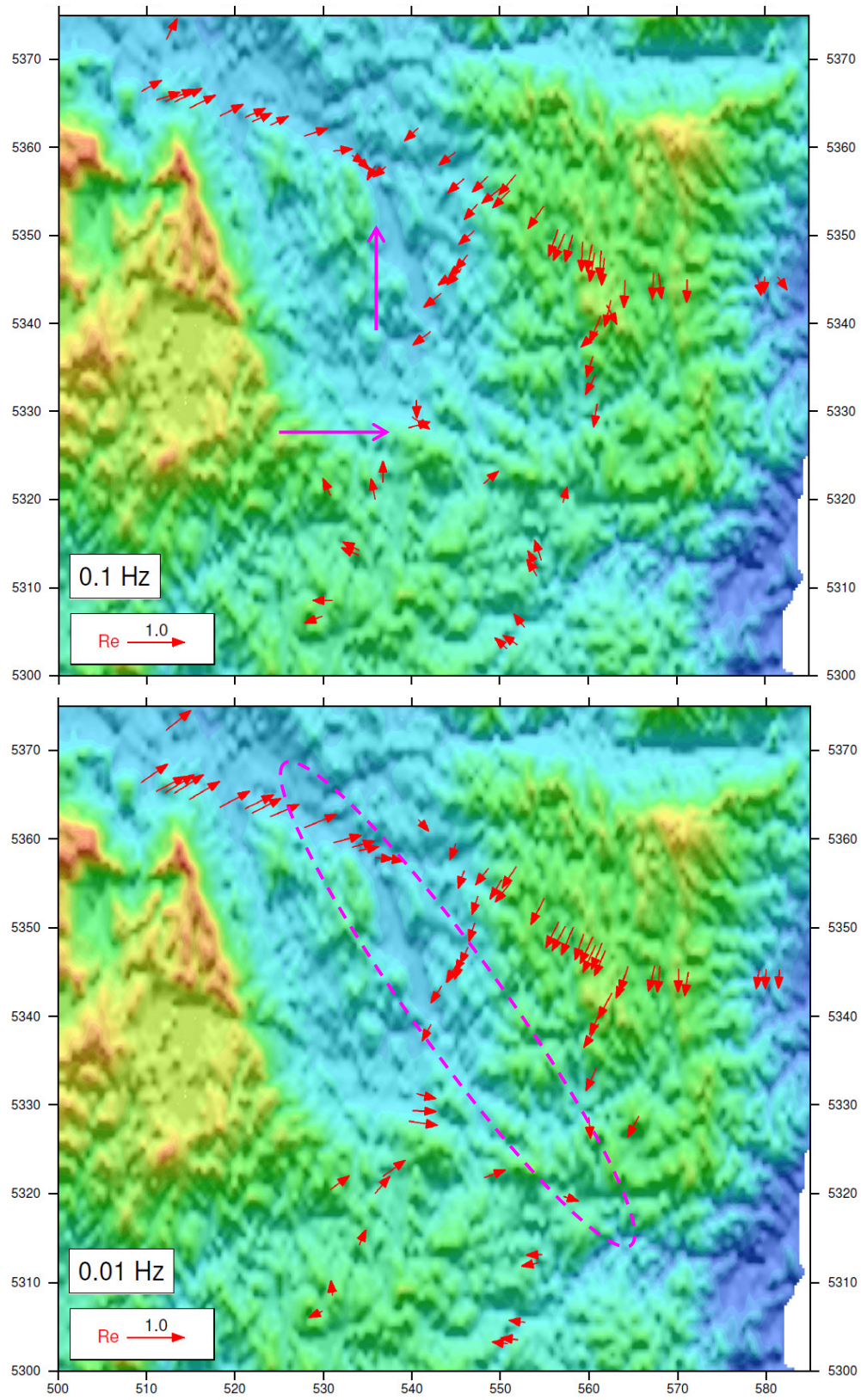


Figure 7: Real induction vectors for 1Hz, 0.1Hz and 0.01Hz (top to bottom). Arrows are plotted in the convention pointing *towards* conductors. Pink arrows added to the 1Hz display show how high conductivity is indicated at major fault locations. The dashed ellipse roughly marks the location of deep high conductivity as indicated by the vectors.



## 2.4 MT Impedance maps and pseudo-sections

Apparent resistivity maps are not presented here due to the prevalent static distortion effects described above, not usually present in the phase. Gridded impedance phase invariants are displayed in Figure 8. Note that due to the uneven site distribution the gridded phase values may not be representative between sites, particularly at high frequencies.

There is generally much lateral and vertical (frequency) variation in the data set. In the north-western section, high phase values at highest frequencies (here: 100Hz) indicate a continuous conductor at relatively shallow depth. In the same area, one decade frequencies lower show low phases show a conductive to resistive transition, i.e. indicate a resistor with increasing depth (10Hz). At intermediate and low frequencies, a NW-SE conductive band at greater depth is marked by a high phase ridge, in accordance with tipper information a longer periods. At longer periods, high phases in the southernmost section hint very deep conductors in this area. At even longer periods (0.01Hz), the ocean effect becomes visible at the westernmost sites (not shown).

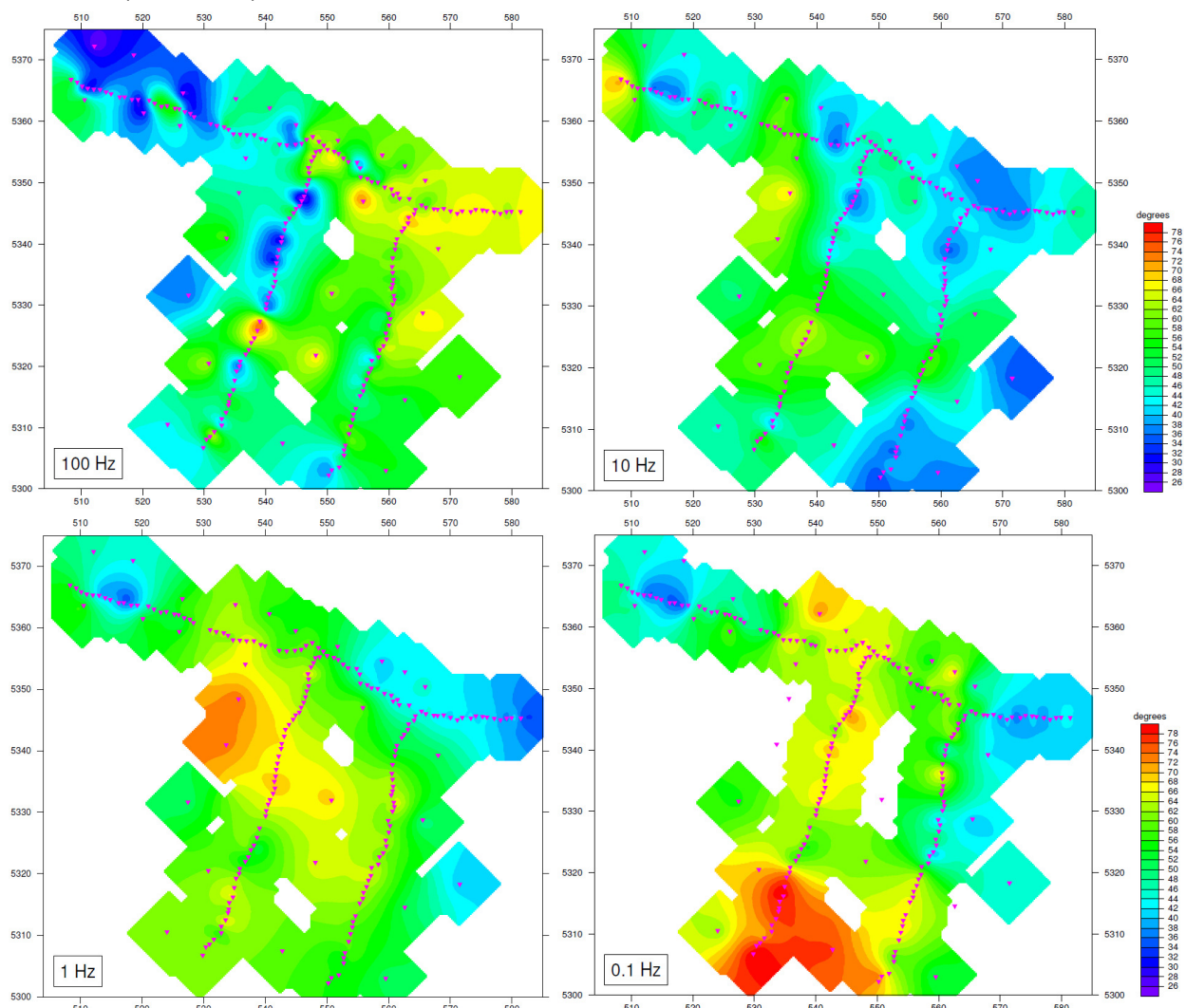


Figure 8 Impedance phase Invariant for frequencies 100Hz, 10Hz, 1Hz, and 0.1Hz.

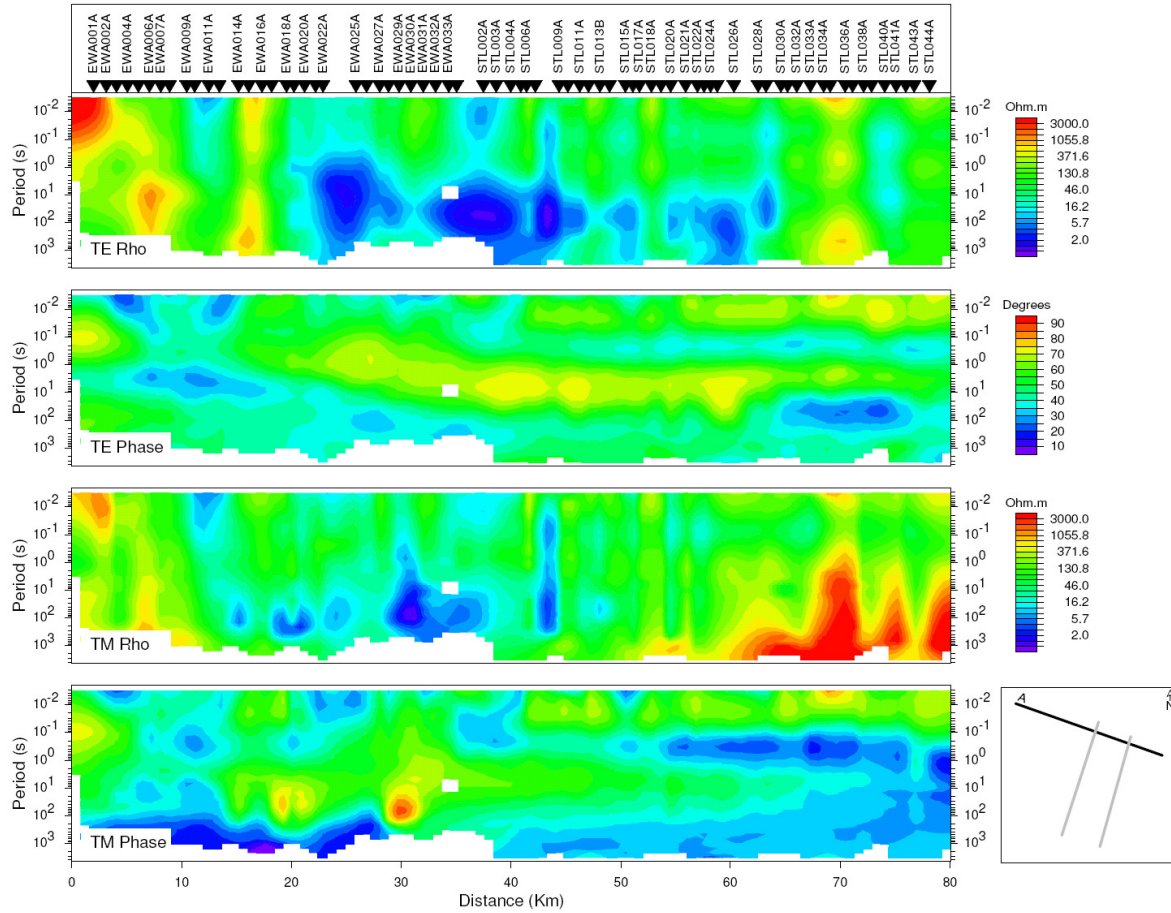


Figure 9 Apparent resistivity and phase pseudo-sections for profile A. Top: TE mode, bottom: TM mode. Data rotation is N18°E, i.e. TE corresponds to electric crossline direction. Vertical stripes in the gridded apparent resistivity data reflect the significant static shifts in the data – lateral phase variation however is smooth. Very low phases and high resistivity at longest periods in the TM polarization is likely at least partly related to the coast effect.

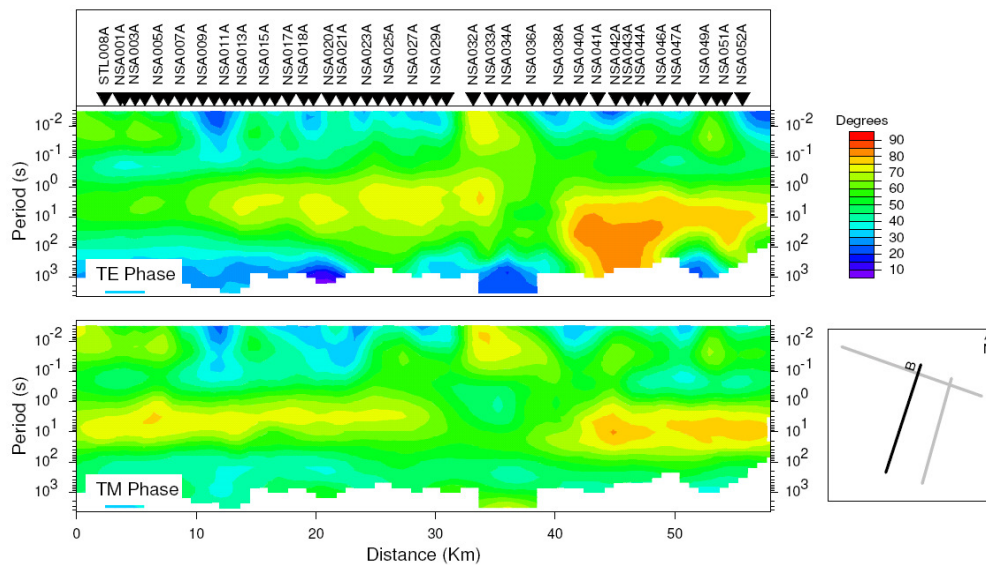


Figure 10 Phase pseudo-sections for profile B for TE (top) and TM polarization (bottom). Data rotation is N-70°E, i.e. TE corresponds to electric crossline direction.

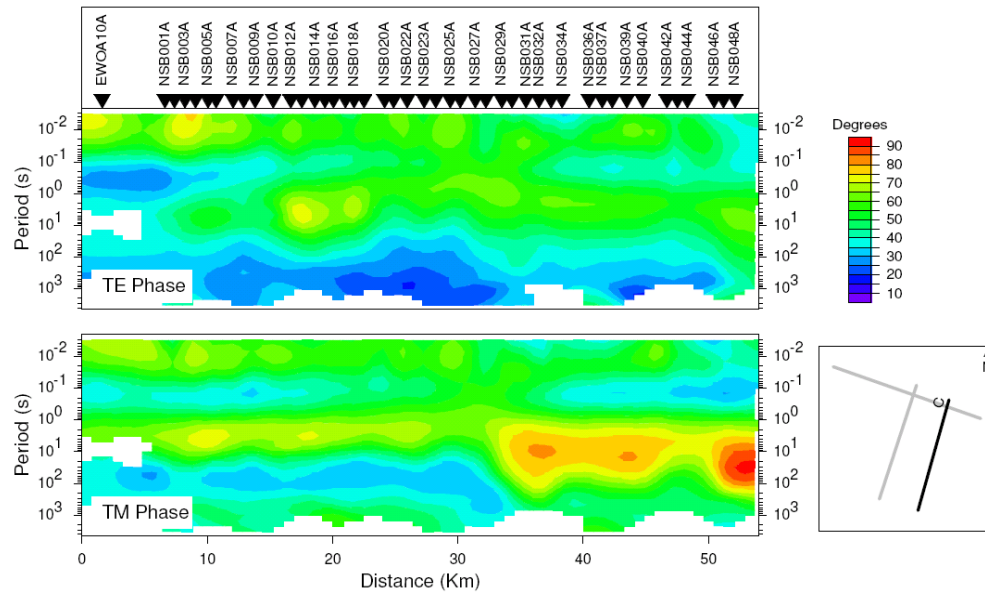


Figure 11 Phase pseudo-sections for profile C for TE (top) and TM polarization (bottom). Data rotation is N-73°E, i.e. TE corresponds to electric crossline direction.

## 3 3D MODELING

Full Tensor MT 3D inversion modelling, including topography and bathymetry, was carried out using the code described by Mackie and Madden (1993) subsequently developed and implemented by Geosystem. The regularization operator produces a smoothly varying resistivity volume, consistent with the gradual resistivity changes expected within a geothermal system. A summary of the 3D modelling technique is given in Appendix B.

### 3.1 Mesh dimensions

Two sets of 3D inversions were run: a fine mesh using all sites, and a coarser mesh using an approximately evenly spaced subset of sites (62 soundings). Both 3D meshes are oriented E16°S (direction of the positive X-axis), and extend considerably beyond the immediate area of interest (horizontally and vertically) in order to avoid model boundary issues (Figure 12 and Figure 13). On the other hand the dimensions of the mesh (number of cells) need to be designed in order to achieve a result in reasonable computation times but with sufficient accuracy.

The set of fine inversion models used the following mesh dimensions:

- horizontal cell size: 800m x 800m in the core area
- vertical cell size : a minimum of 30m for the range of topography, increasing to 100m, constant down to -4,700m elevation.
- total model dimension: 353km × 335km laterally, 74km vertically.
- number of cells: 121×99×112 in X, Y and Z dimensions respectively.

Inversion on the coarser model grid:

- horizontal cell size: 1,500m x 1,500m in the core area
- vertical cell size : a minimum of 50m for the range of topography, increasing to 150m, constant down to -10,000m elevation.
- total model dimension: 593km × 575km laterally, 113km vertically.
- number of cells: 75×64×119 in X, Y and Z dimensions respectively.



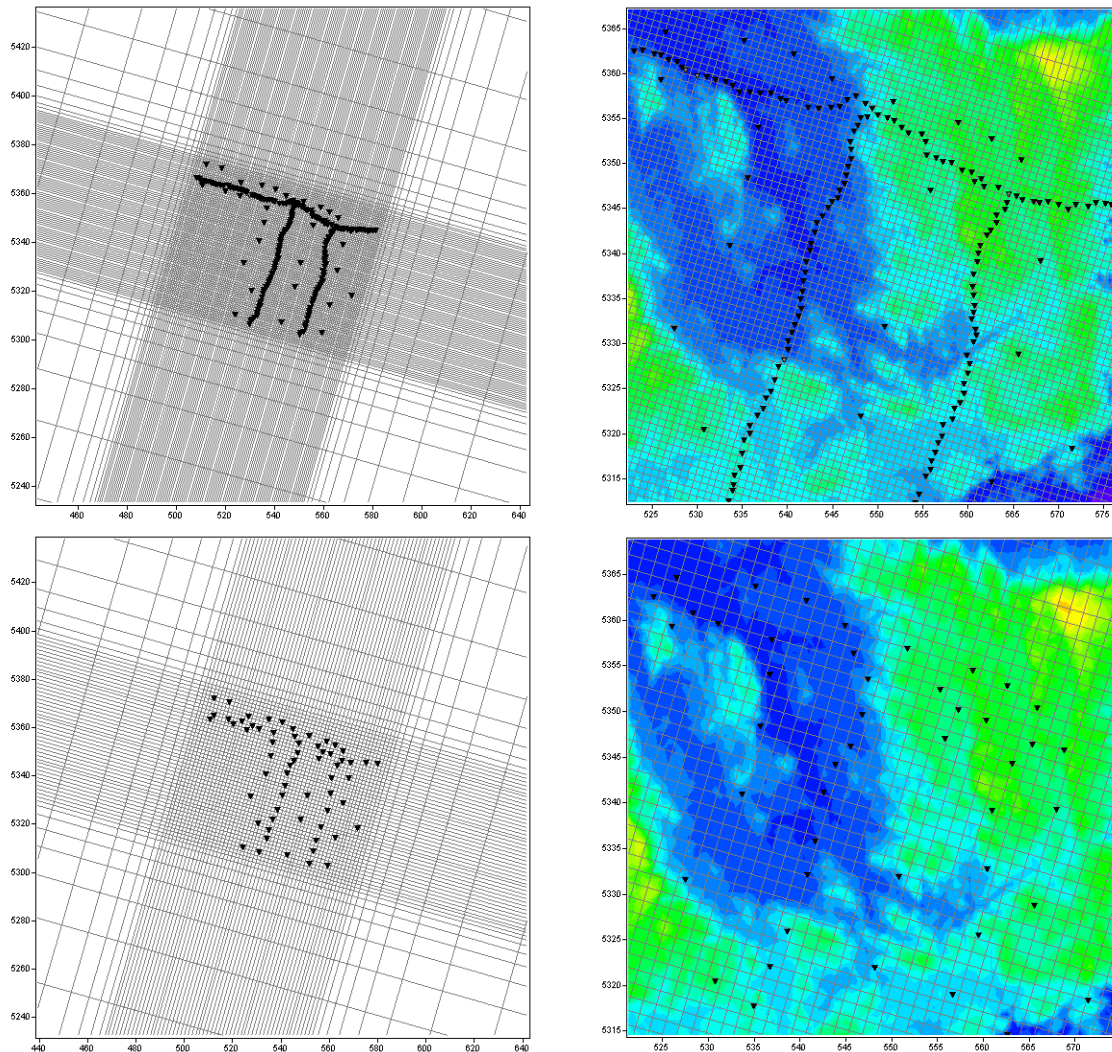


Figure 12. Plan views of full 3D model meshes (LHS) and fine mesh centred on MT station locations (RHS). Background grid is topography (SRTM DEM). The top row shows the fine 3D inversion grid, the bottom the coarser grid.

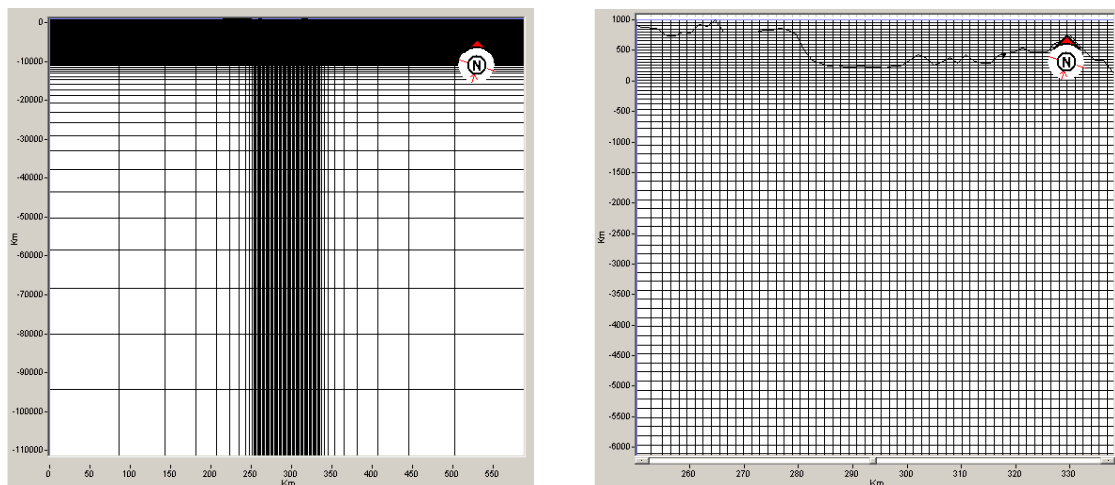


Figure 13 Section views of full and core 3D model mesh (LHS, RHS), showing also the intersection with the elevation grid (RHS; fine model mesh shown here only).

### 3.2 Topography and Bathymetry

The 3D mesh and computations included the topography from a 30m digital elevation model, extracted from SRTM (Shuttle Radar Topography Mission), essential practice in this area were site elevations vary from about 150m to 750m, and the model taking into account also higher and lower elevations as present in the elevation grid. To avoid computational errors the mesh was checked for isolated cells above the topography before running the models.

The easternmost site is about 10km distant from the coastline. Bathymetry taken from the ETOPO1 data set is shown in Figure 14 together with SRTM topography. Water depth on the shelf eastwards does not exceed 150m before about 50km distance from the eastern survey limit, where the continental shelf descends steeply, and reaches below 4000m at about 120km distance.

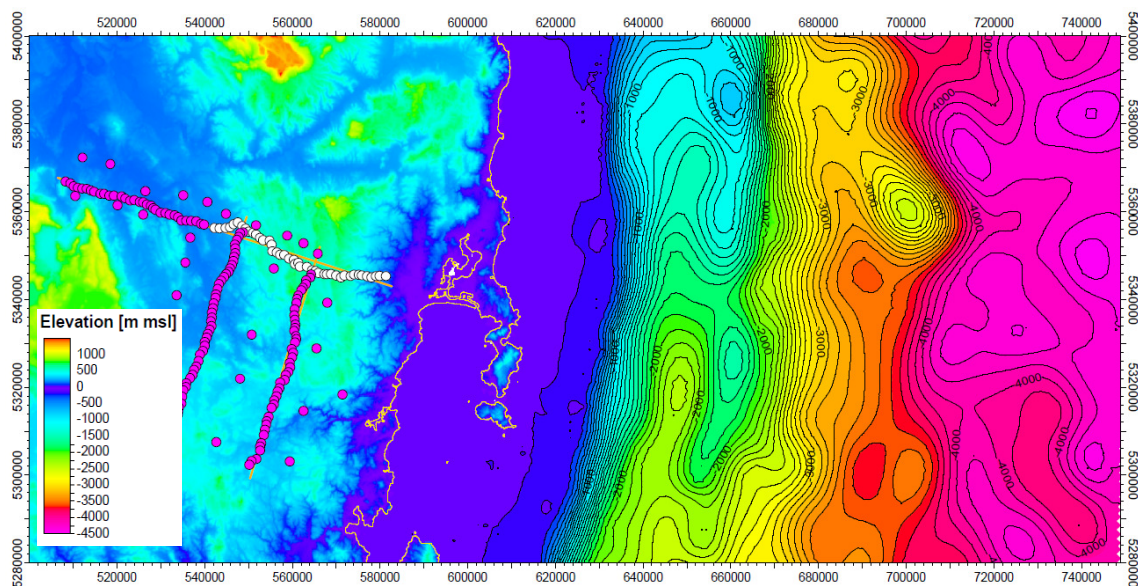


Figure 14 MT station locations and bathymetry.

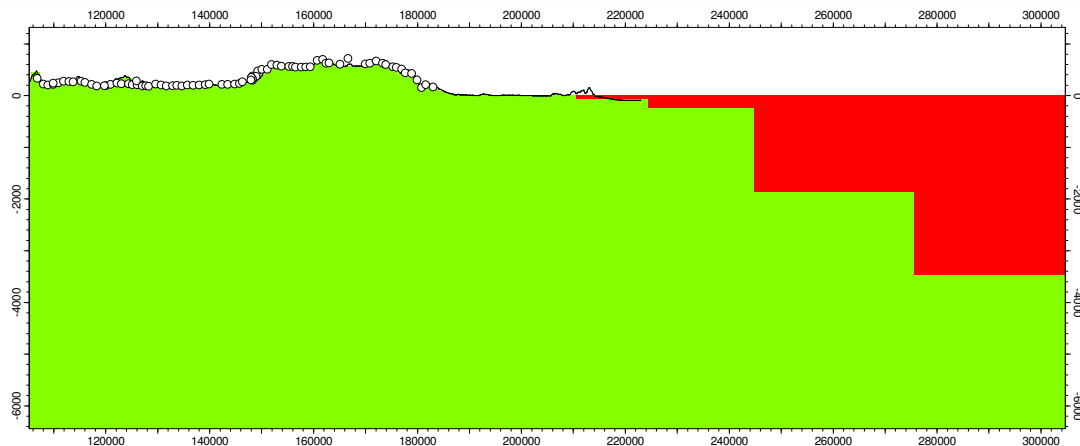


Figure 15 Cross-section through start model of MT inversion. The ocean is coarsely discretized in the eastern padding part of the model.

### 3.3 Inversion parameters

Several, separate 3D inversions were run; varying model parameters to achieve a stable result whilst aiming to minimize the RMS misfit (see Appendix B for a detailed list of inversion settings). The data runs successively verified that after editing, no soundings were causing “single point” biasing of the 3D model. Following this, model smoothness and regularization were varied, controlled by parameters *tau*, *alpha*, and *beta* (horizontal vs. vertical structure weighting). With lower *tau* the model is freer to satisfy local data misfits and reduce the overall RMS misfit, but at the expense of introducing undue roughness and anomalous, extreme resistivity nodes.

The frequency range and number of frequencies used per decade influence the depth range controlled by the model and the model detail respectively. For the fine grid, the final model ran over the frequency range 0.003 to 300 Hz, with 4 frequencies per decade (total 21 frequencies), for the coarser grid, the frequency range was slightly shifted to 0.001 to 100Hz with the same density. Models converged to a stable solution, with a regularization parameter *tau* of 3 for the fine, and 1 for the coarser grid. Magnetic tipper data *was included* in the final inversions.

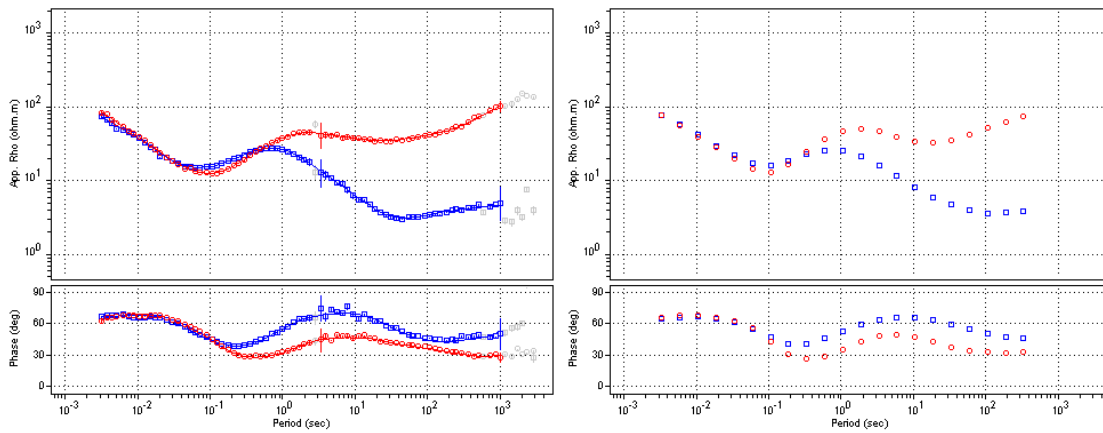
Static shift factors for the off-diagonal impedance elements *Zxy/Zyx* were additionally inverted, setting a dumping constraint, preventing early static shift adjustments at earliest iterations and solving for structure first. The dumping factor gets reduced with increasing iterations. A second constraint controls the overall variance of static shift factors throughout the data set.

The misfit is defined in terms of the rms error, following:

$$\text{rms error} = \sqrt{\frac{1}{npts} \sum \frac{(obs - pred)^2}{var}},$$

where *obs* and *pred* are the observed and predicted data responses (real and imaginary impedance tensors elements over the frequency range used and the stations employed in the inversion), *npts* is the number of data points, and *var* is the defined variance. From this, it is clear that decreasing the variance (i.e. the error floors) has the effect of increasing the rms misfit, and vice-versa. For the final inversion, error floors of 3 and 20 per cent were used for *lnZxy/yx* and *Zxx/yy*, respectively. The RMS misfits for each sounding, together with other model and response files are provided on CD in Appendix D. Examples of computed vs. observed responses are shown in Figure 16.

STL022A, RMS=1.77



NSB034A, RMS=2.07

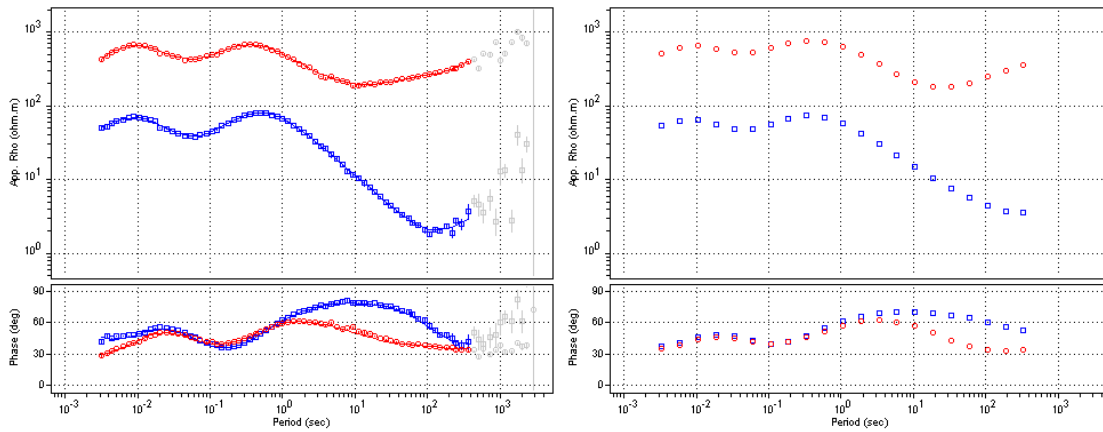


Figure 16 Example MT soundings STL022A and NSB034A, showing fit between observed (LHS) and calculated 3D model response (RHS). Data rotation: 106°. Note the final resistivity model reproduces the static shifts inherent in the MT data at NSB034A, both through inclusion of near-surface structure and direct static shift factors.



## 4 3D MODEL RESULTS

Fine and Coarse models are compared in representative resistivity depth maps for elevations 0, -1500 and -3000 meters in Figure 17.

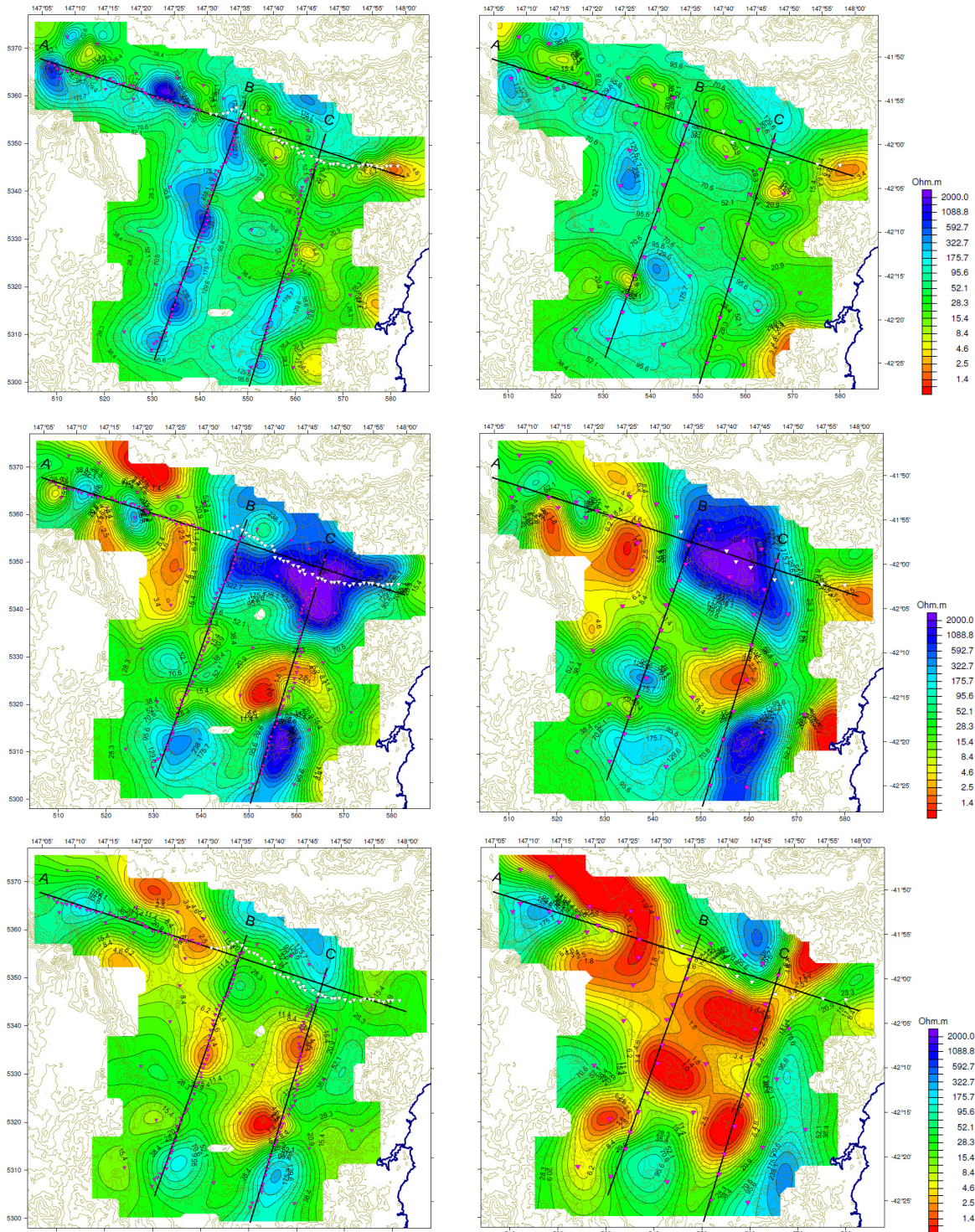


Figure 17 Resistivity depth maps at 0, -1500 and -3000m msl from 3D MT inversion model 06 (fine grid, left panels) and model 102 (coarse grid, right panels).

Cross-sections through the model along profiles A, B, and C are presented in Figure 18 to Figure 20.

While the fine mesh provides reliable *lateral* structural detail below around 500m depth, the extra degrees of freedom near surface, where there is little data control between MT stations, obviously, shallow resistivity artefacts are centred on each sounding (e.g. see depth slices for 0 and 1500m msl. The alternative coarser 3D model mesh gains smoother inter-station continuity near surface, but this sacrifices detail at the depths of interest.

A NW-SE high conductivity band, perhaps linked to fault zones and to the TCZ (Tamar Conductivity Zone), is correlated to induction vectors (Figure 7) and noted in resistivity cross-sections (Figure 18 to Figure 20). The coarse grid model shows the conductive feature smoothed in depth with non-uniform distribution even in the centre of the survey, mainly 3000m depth. Fine grid model display more structural details where station distribution is more defined. This conductivity band has possibly a deep conductive root as shown in both cross sections and resistivity depth maps.

#### ***4.1 Note on fill-in MT data acquisition to improve 3D model***

The resistivity anomalies imaged in the 3D inversion between the detailed profiles MT would certainly benefit from future MT acquisition infill; in particular the lateral geometry constraint, but by association also the vertical distribution. The off-line definition of features presently defined along the profiles will sharpen up, and remove uncertainty in their interpretation.

The inclusion of Tipper data at any future MT sites is encouraged, given this has sensitivity to the target vertical conductive features.

The ideal 3D grid, of course, would aim for an even distribution between the existing profiles, but land access and/or budget constraints seldom facilitate this approach. Given the target interest is somewhere below 2km down, we would suggest 2km 3D grid fill-in directly in the zone of maximum interest, stretching to 3-4km over the remaining 3D model area. The present fill-in is on an 8-10km grid.



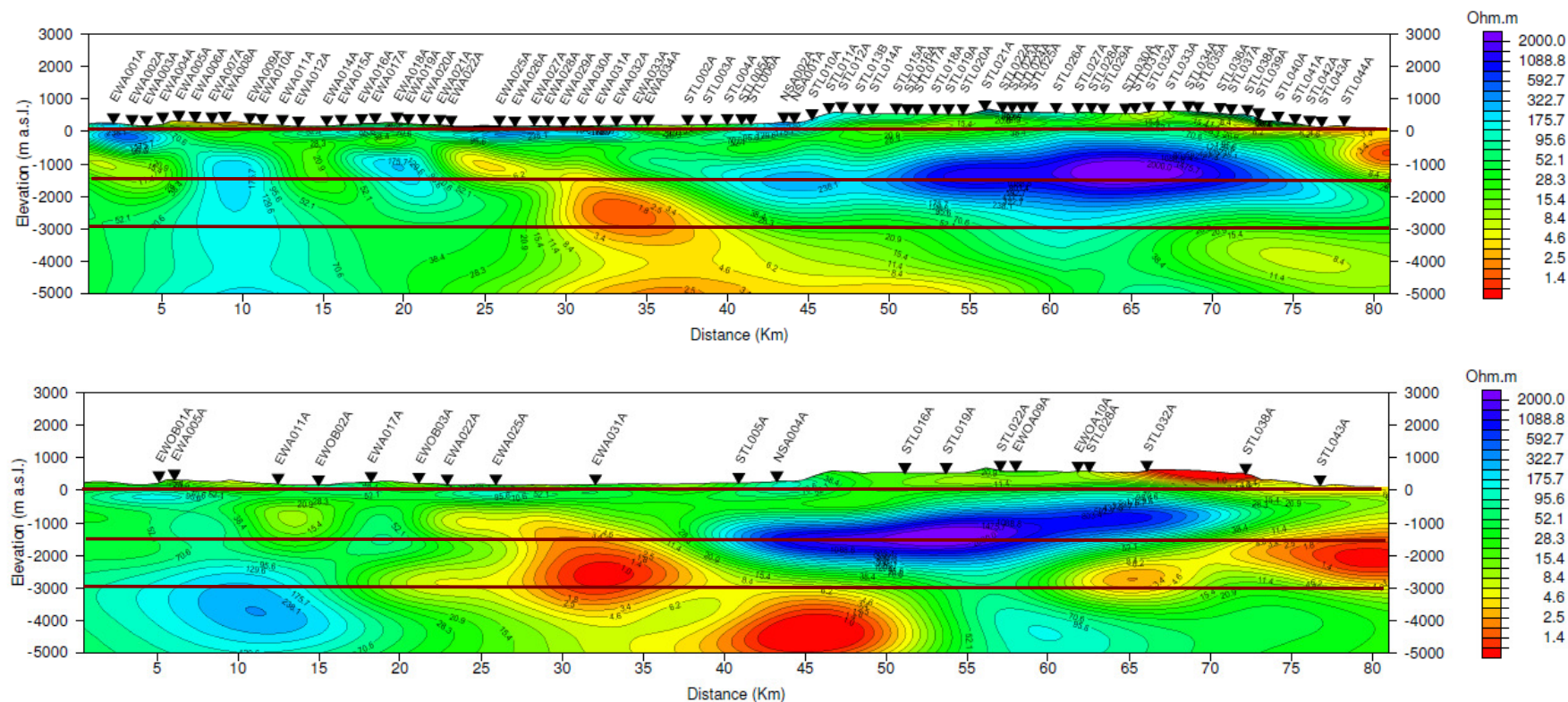


Figure 18 Cross section along profile "A" through the 3D resistivity model 06 (fine grid, W to E, top) and model 102 (coarse grid, W to E, bottom).

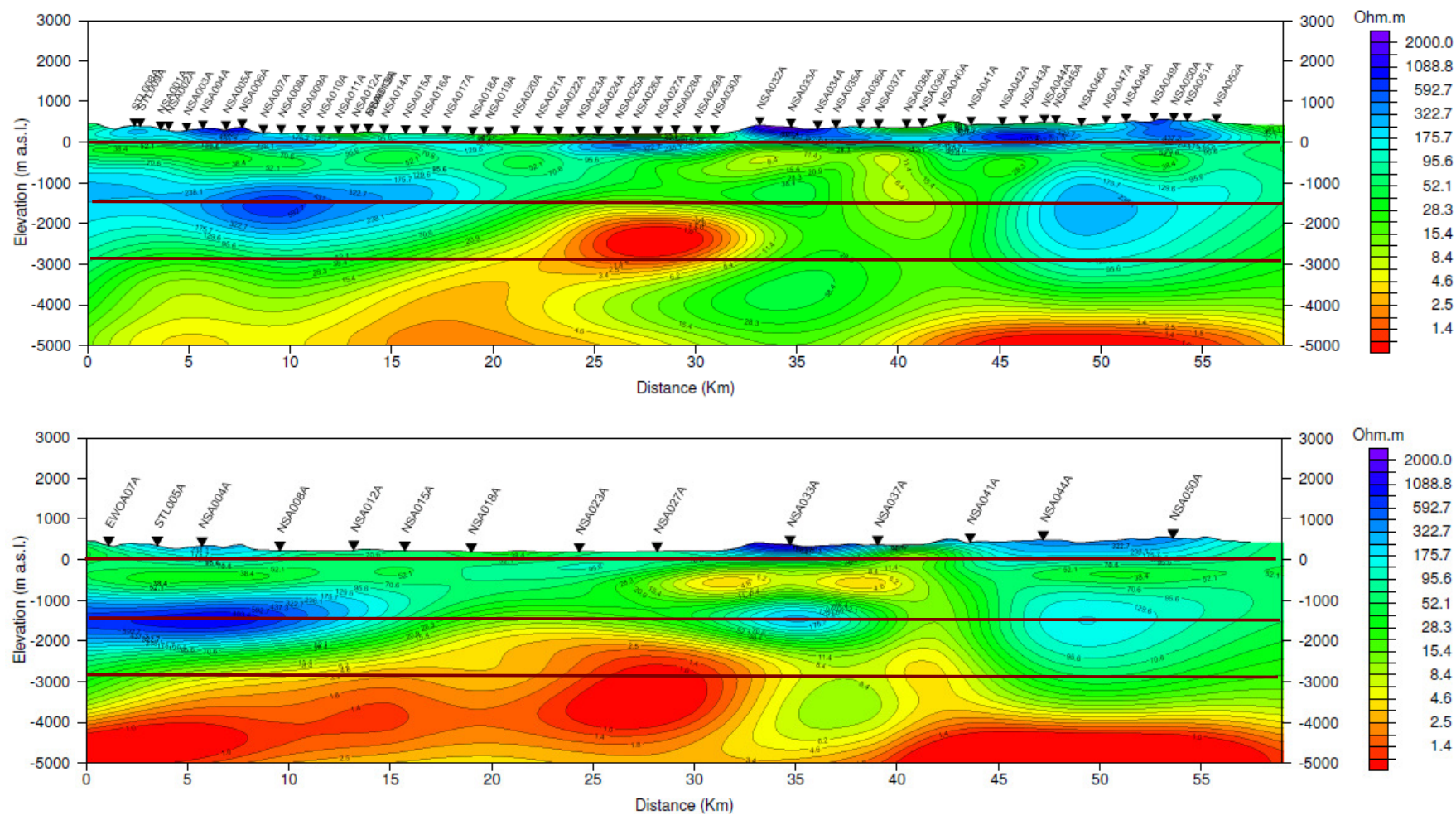


Figure 19 Cross section along profile "B" through the 3D resistivity model 06 (fine grid, W to E, top) and model 102 (coarse grid, W to E, bottom).



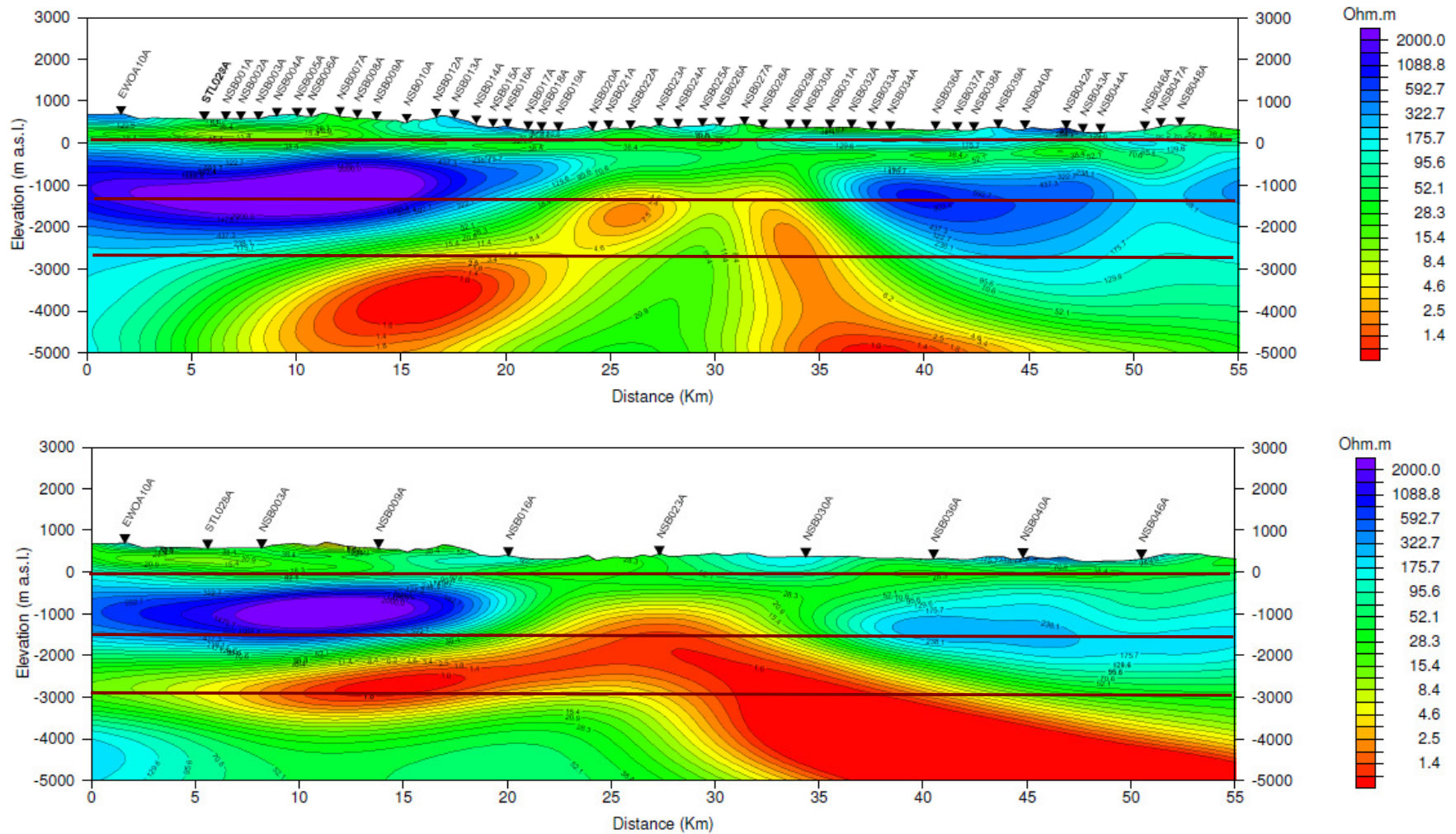


Figure 20 Cross section along profile "C" through the 3D resistivity model 06 (fine grid, W to E, top) and model 102 (coarse grid, W to E, bottom).

## 5 BIBLIOGRAPHY

- |  |      |  |
|--|------|--|
| Andrieux, P. and Wightman, W. E.                                   | 1984 | The so-called static corrections in magnetotelluric measurements, <i>54th Ann. Internat. Mtg. Soc. of Expl. Geophys., Session:EM1.1.</i>   |
| Beamish, D., and Travassos, J.                                     | 1992 | The use of D+ in Magnetotelluric interpretation: <i>J. Appl. Geophys</i> <b>29</b> , 1-19.   |
| Cull, J.P.   | 1991 | Heat Flow and Regional Geophysics in Australia, <i>in</i> Terrestrial Heat Flow and the Lithosphere Structure, Cermak, V. and Rybach, L. (Eds.), <i>Springer-Verlag</i> , 486-500. |
| deGroot-Hedlin, C., and Constable, S.                              | 1990 | Occam's inversion to generate smooth, two-dimensional models from magnetotelluric data, <i>Geophysics</i> , <b>55</b> , 1613-1624.   |
| Fletcher, R. and Reeves, C.M.                                      | 1959 | Function minimization by conjugate gradients, <i>Computer J.</i> , <b>7</b> , 149-154.   |
| Mackie, R.L., and Madden, T.R.                                     | 1993 | Three-dimensional magnetotelluric inversion using conjugate gradients: <i>Geophys. J. Int.</i> , <b>115</b> , 215-229  |
| Mackie, R.L., Rodi, W., and Watts, M.D.                            | 2001 | 3-D magnetotelluric inversion for resource exploration: paper PF3.3, <i>Extended Abstracts, Ann. Mtg. SEG</i>  |
| Polak, E.  | 1971 | Computational Methods in Optimization: A Unified Approach, Academic Press, New York.   |
| Press, W.H., Teukolsky, S.A., Vetterling, W.T., and Flannery, B.P. | 1992 | Numerical Recipes in FORTRAN: The Art of Scientific Computing, Second Edition, Cambridge University Press.   |
| Rodi, W., and Mackie, R.L.   | 2001 | Nonlinear conjugate gradients algorithm for 2-D magnetotelluric inversion, <i>Geophysics</i> , <b>66</b> , 174-187.  |
| Smith, J.T., and Booker, J.R.                                      | 1991 | Rapid inversion of two- and three-dimensional magnetotelluric data, <i>J. Geophys. Res.</i> , <b>96</b> , 3905-3922.   |
| Soyer, W., Hallinan, S., Mackie, R.L., and Cumming, W.             | 2008 | Statics in Magnetotellurics - Shift or Model?, 70th EAGE Conf. & Exhibition, Rome, June 9-12, 2008, extended abstract D020.  |
| Tikhonov, A.N., and Arsenin, V. Y.                                 | 1977 | Solutions of Ill-Posed Problems, V.H. and Sons: Washington, D.C.   |
| Vozoff, K.   | 1991 | The magnetotelluric method <i>in</i> Electromagnetic <i>Methods in Applied Geophysics</i> , Vol2B 641-711, pub. SEG.   |
| Wannamaker, P.E., Hohmann, G.W., and Ward, S.H.                    | 1984 | Magnetotelluric responses of three-dimensional bodies in layered earths, <i>Geophysics</i> , <b>49</b> , p. 1517-1533.   |
| Zhdanov, M.S.  | 2002 | Geophysical inverse theory and regularization problems: Elsevier, <i>Methods in Geophysics</i> 36.   |

## APPENDIX A GLOSSARY

1D	The earth is assumed to be made up of homogeneous horizontal layers
2D	Geology is assumed to be uniform along strike, but varies in the dip direction.
3D	Geology varies in all 3 directions (x, y, and z)
bgl	Below ground level
bsl (asl)	Below sea level (above sea level)
Coils	Sensors used to measure time-varying magnetic fields
Conductance	For a layer, product of layer thickness $\times$ conductivity (Siemens, S). See also Total Conductance, below.
Conductivity	1/resistivity (in S/m).
Contact resistance	Resistance of the electrode pot relative to a ground, measured in $\Omega$ .
E-line	Cable used to measure the electric field
EM	Electromagnetic
$E_x$ and $E_y$	Electric field strengths, in units of mV/km, measured in the x and y directions respectively.
$f$	frequency, in Hertz (Hz)
$H_x$ , $H_y$ , and $H_z$	Magnetic field strengths, in units of nT, measured in the x, y, and z directions (z positive upwards).
Induction arrow	Real part of the vector $\begin{bmatrix} T_x & T_y \end{bmatrix}$ , illustrating the relation between the vertical and horizontal magnetic field components from $H_z = T_x H_x + T_y H_y$ , plotted to show direction towards an assumed 2D line-source (i.e. towards the conductor in the so-called reversed convention).
LaToracca skew angle	$=90^\circ - (\theta_{EH})$ , where $\theta_{EH}$ is the angle between the major axes of the E and H polarization ellipses. Since this angle, should be $90^\circ$ , the La Toracca skew angle should be zero under 1 or 2 D conditions. In 3D conditions, the E field may be distorted (i.e. rotated), resulting in non-zero values.
m msl	meters above Mean Sea Level
Mode (TE or TM)	In a 2D world, the AMT/MT impedance is decomposed into two orthogonal components parallel (TE, or Transverse Electric) and perpendicular (TM, or Transverse Magnetic) to strike. In 1D and 3D situations the definition has limited value.
Occam inversion	Inverse modeling of geophysical data in which no <i>a priori</i> assumptions (e.g. the resistivity/thickness distribution) are made. Rather, the simplest model consistent with the data is found. Named for the 14th century philosopher William of Occam (see Occam, 1324, <i>Quodlibeta</i> , Book V: "Plurality is not to be assumed without necessity").
Period	Inverse of frequency (1/f). Commonly used instead of frequency in describing the low frequency range in AMT/MT (defined in seconds, s)
Pot	Potential electrode: sensor at the end of the E line for measuring the electric field
$\rho$	apparent resistivity in $\Omega m$
$\rho_{max}$ and $\phi_{max}$	The higher of the two apparent resistivity curves and its associated impedance phase.
$\rho_{xy}$	apparent resistivity calculated from $E_x$ and $H_y$
$\rho_{yx}$	apparent resistivity calculated from $E_y$ and $H_x$

RMS error		$\sqrt{\frac{1}{npts} \sum \frac{(obs - pred)^2}{var}}$ <p>where <i>obs</i> and <i>pred</i> are the observed and predicted data responses (real and imaginary impedance tensors elements over the frequency range used and the stations employed in the inversion), <i>npts</i> is the number of data points, and <i>var</i> is the defined variance.</p>
Roughness (of resistivity model)	3D	<p>This is defined as the integral over the 3D model of <math>L^T L \cdot m</math>, where <i>L</i> is the Laplacian and <i>m</i> is the model resistivity. Interfaces in the resistivity are indicated in the model volume by zero-crossings in Roughness. In that this parameter is a fourth derivative, it is inevitably prone to noise, but in compensation aids in identifying the most likely position of an interface.</p>
Sensitivity Matrix, $A^T A$		<p>The sensitivity matrix <math>A^T A \equiv \frac{\Delta(response)}{\Delta(model)}</math> represents the amount of change in the modeled data due to a small change in the model parameter. This shows the sensitivity of the response to a particular 3D model, for each cell of this 3D mesh.</p>
Static shift		<p>Frequency-independent shift of AMT/MT apparent resistivities along the resistivity axis, caused by local electric field distortion.</p>
Static stripping		<p>A method of correcting static shift. At a user-selected (normally high) frequency the impedance is forced to a uniform 1D solution at the actual rotation angle, such that <i>xy</i> and <i>yx</i> apparent resistivities have identical absolute values. The corresponding e-field correction is then applied for all frequencies, and impedance re-calculated at the same orientation angle. Stripping therefore attempts to correct static shift via the impedance distortion, rather than simply block-shifting the (derived) apparent resistivity curves.</p>
TD		<p>Total depth (of a well).</p>
Tipper		<p>Ratio of the vertical magnetic component <math>H_z</math> to the horizontal magnetic field components <math>H_x</math> and <math>H_y</math>. Since the vertical component (noise excluded) is the output of a system (the earth) to which the two horizontal components are the input, its absolute value should not exceed 1 (see <i>induction arrow</i>).</p>
Tipper strike		<p>The geographic orientation in the horizontal plane of the vector relationship between the magnetic field components (<i>tipper</i>), taking real and imaginary parts into account. In a 2D earth, the tipper strike is perpendicular to the induction arrow direction, and shows the um 2D geo-electric strike.</p>
Top of conductor		<p>A surface interpreted from a resistivity distribution (e.g. 1D layered earth models or 3D resistivity volume in the MT case ) depicting the elevation of the top of the (principal) conductive horizon. Shown as contour map or line on cross-section. Units are m msl.</p>
Total conductance		<p>The conductivity (=1/resistivity), integrated to a specified depth <i>z</i>:  <math display="block">TC = \sum_0^z \Delta z_i / \rho_i</math> , where <math>\Delta z</math> is the thickness of the <i>i</i>th layer and <math>\rho_i</math> its resistivity.</p>

## APPENDIX B 3D MT INVERSION

### ***B.1 AN INTRODUCTION TO 3D MT INVERSION***

The general approach to the inversion of geophysical data consists of two steps: (1) the computation of a forward response, and (2) the comparison of this with observed data, and modification of the starting model in light of the differences between observed and computed data. To be reasonably practical, this requires a fast forward code and an efficient approach to inversion.

### ***B.2 3D FORWARD MODELING***

3-D MT data are derived from measurements at Earth's surface of naturally occurring electric and magnetic fields. A standard 3-D MT dataset usually comprises four complex quantities (impedances) as a function of receiver position and frequency. The four impedances observed in 3-D MT, then, are the components of a  $2 \times 2$  impedance tensor. Modeling of the impedance tensor entails solving Maxwell's equations in the solid earth and atmosphere using a horizontal current source in the atmosphere to represent ionospheric and magnetospheric sources. In our modeling algorithm we divide the earth and atmosphere into rectangular blocks with the magnetic fields defined along the block edges and the electric fields defined along the normals to the block faces (Mackie et al., 1994). Finite difference equations can be easily derived using this formulation. If one eliminates the electric fields from the difference equations, one obtains a second-order set of equations in  $H$ . This system of equations is sparse, symmetric, and complex (all elements are real except for the diagonal elements). The solution to this system is obtained by use of the stabilized biconjugate gradient algorithm. Convergence is speeded up by use of a preconditioner that is the incomplete Cholesky decomposition of the diagonal sub-blocks with fill-in plus a correction for the divergence of the magnetic field (Mackie et al., 1994). Once the  $E$  and  $H$  fields have been determined for two linearly-independent source polarizations, the impedance tensor can be computed.

### ***B.3 3D INVERSION***

The general magnetotelluric inverse problem is posed in canonical form and solved using the framework of Tikhonov regularization (Tikhonov and Arsenin, 1977). Following many previous workers in MT inversion, a smooth, or 'minimum-structure', resistivity model that gives acceptable fits to the observed data is sought. Thus, using a simple second-order operator, solutions are models with minimum spatial variability, or roughness. The method of nonlinear conjugate gradients (NLCG) is used to minimize the misfit; nonlinear conjugate gradients are a well-known optimization method (Fletcher and Reeves, 1959) which has been applied in a variety of nonlinear geophysical inverse problems, e.g., Ellis and Oldenburg (1994). While NLCG is a general method for optimization, it is not necessarily efficient in a computationally intensive problem like 2-D and 3-D MT inversion. The efficiency of NLCG for computing solutions of the inverse problem depends strongly on the preconditioner and the line

minimization algorithm. The purpose of these is to steer the gradient into a direction in model space which parallels the final solution as much as possible. A restriction on this goal is that applying the preconditioner can require an excessive amount of computation if it is too complicated. It is applied to a parameter vector by solving the linear system, which can therefore be applied efficiently, acting in some sense like the inverse Hessian matrix. The amount of computation needed to solve the system is less than one forward function evaluation and thus adds little overhead to the algorithm. Line minimization is only a one-dimensional problem, requiring the computation of at least one forward problem, which in 3-D MT is computationally demanding. It is thus very important to use an algorithm that does a reasonable job in the current search direction with as few trials as possible. Algorithms such as that in Press et al. (1992) do not achieve this goal. In our 3-D MT algorithm, we use a line minimization algorithm that is basically a univariate version of the Gauss-Newton method. While details of this algorithm are given in Rodi and Mackie (2001), the important result of this algorithm is that each step of the line minimization iteration requires the equivalent work of only three MT forward calculations (the real one and two pseudo ones). An additional efficiency is our choice of stopping criterion. It ensures that, when the forward problem is well-approximated by its linear approximation, each line minimization converges in a single step.

The net result is that the observed 3D data (each element of the impedance tensor, at each frequency used) can be inverted to give a smooth 3D model. The method is efficient and generally fairly fast: the final inversion on the fine grid – with a high number of 21 frequencies – took approximately 170 minutes per iteration of CPU time on a parallel cluster with 120 nodes running the Linux operating system. For comparison, the running time was much reduced on the coarser grid with 70 minutes / iteration.

Smooth model inversions are quite useful for geologic interpretations because they provide accurate representations of the subsurface. Their disadvantage, however, is that they do not resolve sharp boundaries or interfaces. Rather, because of the smoothness constraint, interfaces are defined in general terms by resistivity gradients. Practically, however, what is of interest is the depth to a particular interface or geologic formation. In those situations where additional information is available (e.g., well logs, seismic, etc), we can use that information to generate a “tear surface” which we then project onto the MT model. Across this surface, we turn off the smoothing constraint and allow the resistivities to vary independently above and below the surface. If the geology is well approximated by this surface, then the resulting model will in general be smooth except across this surface. In this way, we can introduce sharp boundaries into the 3D MT inversion.

## APPENDIX C PRINCIPAL 3D MODEL PARAMETERS

Setup	iterations	cumulative its	rms	start model	tau	tipper inversion	lnZxy amplitude	lnZxy phase	tipper error floor	reg operator	smoothest variations	static shift	orientation [deg]	nx	ny	nz	min dx, dy [m]	min dz [m]	deep dz [m]	# sites	# frequencies	# freqs / decade	min frequency
01_Aug20	30	30	2.889	fine 20Ωm	3	n	3%	3%		Lapl	n	n	-16	121	99	112	800	30	100	198	21	4	0.003
02_Aug24	20	20	3.350	01_30iter	10	y	3%	3%	0.02	Lapl	n	n	-16	121	99	112	800	30	100	198	21	4	0.003
05_Sep04	20	20	3.209	fine 20Ωm	10	y	3%	3%	0.02	Lapl	n	y	-16	121	99	112	800	30	100	196	21	4	0.003
<b>06_Sep05</b>	30	50	2.398	05_20iter	3	y	3%	3%	0.02	Lapl	n	y	-16	121	99	112	800	30	100	196	21	4	0.003
100_Sep24	30	30	2.975	coarse 20Ωm	10	y	3%	3%	0.02	Lapl	n	y	-16	75	64	119	1500	50	150	62	21	4	0.001
101_Sep24	35	65	2.337	100_30iter	3	y	3%	3%	0.02	Lapl	n	y	-16	75	64	119	1500	50	150	62	21	4	0.001
<b>102_Sep28</b>	30	95	1.969	101_35iter	1	y	3%	3%	0.02	Lapl	n	y	-16	75	64	119	1500	50	150	62	21	4	0.001

The model resulting from inversions 06 and 101 are considered the final fine and coarse resistivity model, respectively.

Cumulative iteration	Inversions involving a re-start (typically with lower tau, see below): total number of iteration considering also the number of previous iterations.
Rms	Root mean square: measure of data fit (see also glossary in Appendix A). Average number of standard deviation between the model data and the observed data
Tau	Regularization parameter that controls the tradeoff between fitting the data and adhering to the model constraint (larger values cause a smoother model at the expense of a worse data fit)
lnZxy amplitude (& phase), Zxx/Zyy	Error floors in % (absolute for tipper). Please not that logarithm has been calculated in the xy and yx cases
Regularization	Regularization operator measuring the model structure/roughness
Tau (m-m0)	Constraint penalizing any deviations from the a-priori model, contributing to the total objective function.
nx, ny, nz	number of cells in the x, y, z direction
min dx, min dy, min dz	minimum cell dimension in the x, y, z direction (in meters)





## APPENDIX D DIGITAL DATA ON CD

### ***D.1 DIGITAL DATA ON CD***

The enclosed CD contains:

#### **WinGLink Database**

WinGLink database, with all MT data and TDEM data and 3D inversion results.

#### **Report**

**Tasmania 3D MT Modeling 2009.pdf:** Acrobat pdf file of this report.

**Plates and Resistivity Cross Sections** from 3D MT inversion (see Appendix E)

#### **3D Inversion Results for both, fine and coarse grids calculations:**

- model file (3dmod.out), with mesh specifications and final resistivity values,
- errors\_d3inv.dat, containing inversion statistics,
- rmsvals.dat, listing the rms misfit for each station,
- predicted data in EDI format

The 3D model mesh, the inversion statistics, the RMS misfit file and the predicted MT response files at each site (EDI files) are as follows:

### ***D.2 OUTPUT DATA FORMATS***

The files associated with the 3D inversions consist of the following:

1. model file (3dmod.out), which contains the mesh specifications and the final resistivity values;
2. errors\_d3inv.dat, which contains inversion statistics;
3. rmsvals.dat, in which the rms misfit for each station is listed;
4. predicted data, in EDI format, that is, the computed impedance responses at each site.

### D.2.1 Model File

This is an ASCII fixed-format file, which begins in the following form:

121	99	112	13	VAL		
.4614E+05	.3076E+05	.2050E+05	.1367E+05	9113.	6075.	4050.
800.0	800.0	800.0	800.0	800.0	800.0	800.0
800.0	800.0	800.0	792.5	807.5	800.0	800.0
800.0	800.0	800.0	800.0	800.0	800.0	800.0

In this, the first three figures indicate the number of cells in the x, y, and z directions, and the following three rows list the cell dimensions in meters. The number 1 (fourth row) is a flag indicating that the resistivity values follow, and these are listed in the order of row (x), horizontal column (y), and depth (z) respectively.

At the end of the file, five lines contain the information needed to locate the mesh on the real world coordinate system.

WINGLINK	
Site_not_set	(site name)
1	1 (i j block numbers)
431.3437	5515.378 (real world coordinates)
-16.00000	(rotation)
1.020000	(top elevation)

The model cell for reference purposes is indicated on the first line, with its coordinates (i, j) relative to the 3D mesh (of which cell 1,1 is in the extreme north-west). The following line gives the coordinates of the centre point of this cell in kilometers on the local reference system (here: WGS84, Transverse Mercator projection).

### D.2.2 Predicted Data

The computed responses are output in separate EDI files (Wight, 1988), one per site. These contain the frequencies and computed impedances corresponding to the final 3D inversion models.

### D.2.3 Inversion Log and Error File

File errors\_d3inv.dat lists the inversion parameters, and, for each iteration, the rms misfit and objective functions. rmsvals.dat lists the final rms misfit between the observed and computed responses at each station.

## APPENDIX E MAPS AND CROSS SECTIONS

The resistivity colour scale is identical for all resistivity maps and cross-sections.

### ***E.1 MAPS***

MT station and profile locations are shown on topographic base map in Plate 1.

The 3D resistivity mesh is illustrated via depth slice maps in Plates 2a-k, from -250m to -5000m msl.

Scale 1:350,000.

### ***E.2 CROSS SECTIONS***

Resistivity cross-sections ( $\Omega\text{m}$ ) from smooth 3D inversions are plotted for main profiles A, B, and C, and three additional profiles (D, EW-1, EW-2) between these.

Horizontal and vertical scales are at 1:250,000 and 1:125,000, respectively. Vertical exaggeration is 2.